Collisions of Slow Polyatomic Ions with Surfaces: The Scattering Method and Results

Zdenek Herman
V. Čermák Laboratory, J. Heyrovský Institute of Physical Chemistry, Academy of Sciences of the Czech Republic, Prague, Czech Republic

Surface-induced dissociation (SID) and reactions following impact of well-defined ion beams of polyatomic cations $C_2H_5OH^+$, CH_4^+, and CH_5^+ (and its deuterated variants) at several incident angles and energies with self-assembled monolayers (SAM), carbon surfaces, and hydrocarbon covered stainless steel were investigated by the scattering method. Energy transfer and partitioning of the incident projectile energy into internal excitation of the projectile, translational energy of products, and energy transferred into the surface were deduced from the mass spectra and the translational energy and angular distributions of the product ions. Conversion of ion impact energy into internal energy of the recoiling ions peaked at about 17% of the incident energy for the perfluoro-hydrocarbon SAM, and at about 6% for the other surfaces investigated. Ion survival probability is about 30–50 times higher for closed-shell ions than for open-shell radical cations (e.g., 12% for CD_5^+ versus 0.3% for CD_4^+, at the incident angle of 60° with respect to the surface normal). Contour velocity plots for inelastic scattering of CD_5^+ from hydrocarbon-coated and hydrocarbon-free highly oriented pyrolytic graphite (HOPG) surfaces gave effective masses of the surface involved in the scattering event, approximately matching that of an ethyl group (or two methyl groups) and four to five carbon atoms, respectively. Internal energy effects in impacting ions on SID were investigated by comparing collision energy resolved mass spectra (CERMS) of methane ions generated in a low pressure Nier-type electron impact source versus those generated in a Colutron source in which ions undergo many collisions prior to extraction and are essentially vibrationally relaxed. This comparison supports the hypothesis that internal energy of incident projectile ions is fully available to drive their dissociation following surface impact. (J Am Soc Mass Spectrom 2003, 14, 1360–1372) © 2003 American Society for Mass Spectrometry

Studies of interaction between hyperthermal ions and surfaces represent a broad area of research of interest to both physicists and chemists. A variety of phenomena and processes is induced in the range of collision energies from eV to keV and higher, and many of them find use in different areas of science and technology [1]. Especially over the last fifteen years, considerable interest has been devoted to studying selected physical and chemical processes stimulated by impact of 5–100 eV ions on surfaces [1–4]. In this energy regime, the relative collision energy is of the same order of magnitude or somewhat larger than the chemical bond energies. The ion-surface interaction is thus large enough to lead to bond dissociation but not to obscure its chemical nature. Collisions of slow ions with surfaces find many applications in science and technology ranging form surface diagnostics, surface modification and preparation of new materials, description of plasma-wall interactions in discharges and fusion devices to characterization of projectile ions. In particular, surface collisional activation and ensuing surface induced dissociation (SID) has been increasingly used as one of the tools for characterizing structural properties of organic (bioorganic) ion projectiles [3, 4]. The question of collisional-to-internal energy transfer has been extensively studied. The average energy transferred was estimated from the extent of fragmentation of the projectiles using different procedures [5–7] or from the fragmentation of "thermometer molecules" [8, 9], exhibiting simple and regular break-down patterns. Valuable information was also obtained from model calculations [8].

$$E_{TOT} = E_{tr} + E_{int} = E'_{int} + E'_{tr} + E'_{surf}, \quad (1)$$

where E_{tr} is the translational energy of the incident projectile, E_{int} is its initial internal excitation, E'_{int} is the

Published online October 23, 2003

Address reprint requests to Dr Herman, V. Čermák Laboratory, J. Heyrovský Institute of Physical Chemistry, Academy of Sciences of the Czech Republic, Dolejškova 3, CZ-182 23 Prague 8, Czech Republic. E-mail: zdenek.herman@jh-inst.cas.cz

1044-0305/03/$30.00
doi:10.1016/j.jasms.2003.09.002

Received May 20, 2003
Revised August 27, 2003
Accepted August 27, 2003

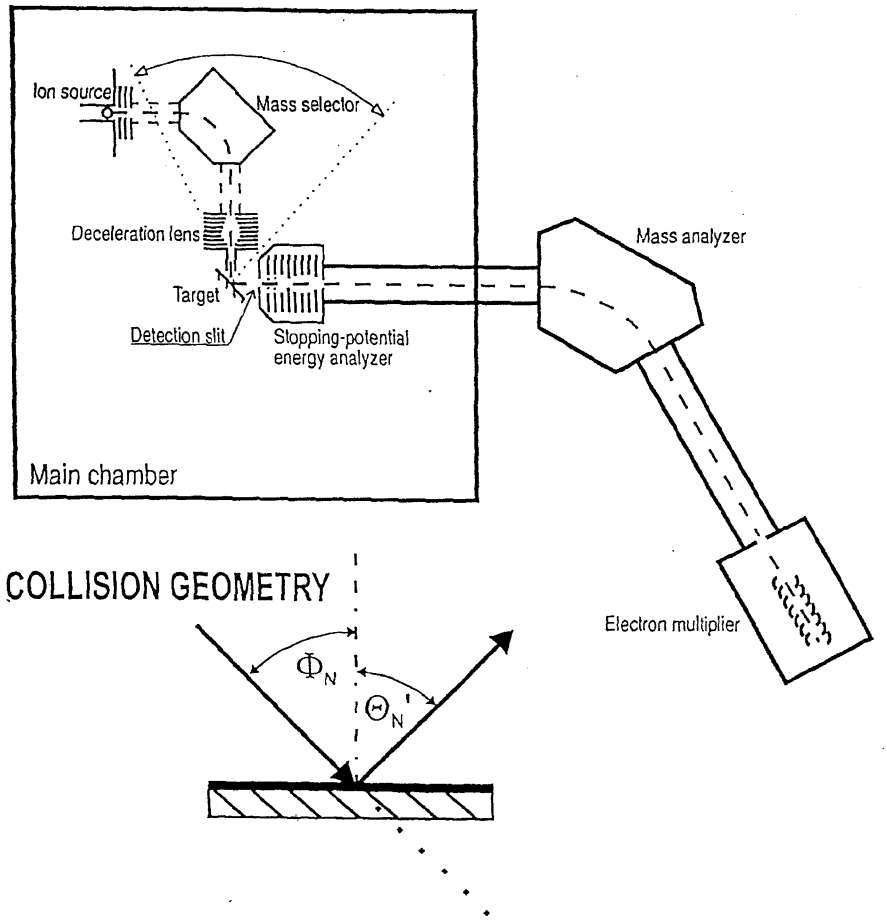

Figure 1. Schematics of the scattering apparatus. Inset defines the collision geometry.

internal energy of the surface-excited projectile ion after the collision, E'_{tr} is the translational energy of the product ions, and E'_{surf} is the energy absorbed by the surface.

This communication is a review of a series of scattering experiments in our laboratory to obtain information on the energy partitioning in surface collisions of slow polyatomic ions [10–14]. This approach uses a combination of measurement of mass spectra, translational energy distributions, and angular distributions of the product ions to obtain data on distributions of energy fractions in eq 1. The data were obtained in dependence on the incident ion energy, on the incident angle, on the type of the surface, and also—in some cases—on the surface temperature.

The surfaces studied were those covered by different types of self-assembled monolayers (hydrocarbons, perfluoro-hydrocarbons, hydrocarbon chains with specific terminal groups), hydrocarbon-covered metal surfaces, and carbon surfaces. The carbon surfaces were investigated both at room temperature and at an elevated temperature of 1000 K.

The projectile ions used were ethanol molecular ion ($C_2H_5OH^+$), and small hydrocarbon ions (CD_3^+, CD_4^+, CD_5^+, and their H- and ^{13}C- isotopic variants). Especially the ethanol molecular radical cation proved to be very useful in the estimation of energy partitioning. It carries a relatively small amount of internal energy from electron impact ionization, its break-down pattern is well known from both experiment and theoretical calculations, and its unimolecular dissociation processes can be easily separated from products of fragmentation of its protonated product, formed in H-atom transfer reactions with surface hydrogen-containing material.

Experimental Method

The beam scattering apparatus EVA II was used in the investigations described here (Figure 1). Projectile ions were formed by bombardment of a source gas in a low-pressure ion source by 120 eV electrons. The ions formed were extracted, accelerated to about 140–300 eV, mass analyzed by a 90° permanent magnet, and decelerated to a required energy in a multi-element deceleration lens. The resulting projectile ion beam had an energy spread of 0.2 eV full-width-at-half-maximum (FWHM), an angular spread of 1° FWHM, and geometrical dimensions of 0.5 × 1.0 mm. The beam was

directed towards the target surface under a pre-adjusted incident angle Φ_N. Ions scattered from the surface passed through a detection slit (0.5 × 1 mm), located 25 mm away from the target, into a stopping potential energy analyzer. They were then accelerated to 1000 eV into a detection mass spectrometer (a magnetic sector instrument) and detected with a Galileo channel multiplier. Both the amplified signal current measurement and ion counting could be used. The projectile beam exit slit, the target, and the detection slit were kept at the same potential during the experiments and this equipotential region was carefully shielded by μ-metal sheets. The projectile beam–target section could be rotated about the scattering center with respect to the detection slit to obtain angular distributions. The use of a simple stopping potential energy analyzer has its advantage in this type of study (e.g., in comparison with deflection analyzers): specifically, it makes it possible to measure mass spectra of the ion products and determine total intensities of scattered ions regardless of their kinetic energy and to measure then their translational energy distributions separately.

The energy of the projectile ions was measured by applying to the target a potential exceeding the nominal ion energy by about 10 eV. The target area then served as a crude ion deflector directing the projectile ions into the detection slit. Their energy could be determined with accuracy better than about 0.2 eV. The impact angle of the projectile ions was adjusted before an experimental series by a laser beam reflection with a precision better than about 1°. Incident (Φ_N) and scattering (Θ'_N) angles were measured with respect to the surface normal (see inset in Figure 1).

The surfaces investigated were self-assembled monolayers on gold-covered silicon wafers ($C_{11}F_n$-SAM, $C_{12}H_n$-SAM, and C_{11}-COOH-SAM), carbon surfaces, [highly oriented pyrolytic graphite (HOPG); samples of carbon bricks from tokamaks], and hydrocarbon-covered polished metal surfaces. The carbon surfaces could be heated up to 1000 K. At room temperature, the carbon surfaces were covered by a layer of hydrocarbons, as manifested by the occurrence of chemical reactions of H-atom and CH_n- transfer between the projectile ion and surface material [14]. Heating this surface to 1000 K effectively removed this hydrocarbon layer: The hydrocarbon concentration decreased to less then 1%, as confirmed by the absence of H-atom transfer reactions. Cooling to room temperature re-established the hydrocarbon surface layer. This cycle could be repeated reproducibly several times and followed by the presence or absence of the products of chemical reactions in the mass spectra. In the early energy transfer experiments the surface was a polished metal (stainless steel, nickel), covered by layer of background hydrocarbons. This is a very stable surface used in many earlier mass spectrometry experiments on surface-induced dissociation of organic ions [2]. The background pressure in the scattering apparatus was about 5×10^{-7} torr, and during experiments the pressure was about 3×10^{-6} torr because of leakage of ion source vapor into the scattering chamber.

Results and Discussion

Energy Transfer in Surface Collisions of Polyatomic Ions

Information on energy partitioning was obtained from measurements of mass spectra and translational energy distributions of the product ions. Figure 2 summarizes results of several such measurements for the CF-SAM (Figure 2a) and CH-SAM (Figure 2b) surfaces and the projectile molecular ethanol ion $C_2H_5OH^+$ at a collision energy of 22 eV and incident angle 132_N of 60° (30° with respect to the surface). Mass spectra in Figure 2a (CF-SAM) measured in the product ion angular maximum show substantial fragmentation of the molecular ion projectile $C_2H_5OH^+$ (*m/z* 46) to $C_2H_5O^+$ (*m/z* 45), to CH_2OH^+ (*m/z* 31), and to a lesser extent to COH^+ (*m/z* 29, nature of the ion proved by isotope labeling). CH-SAM spectra shown in Figure 2b exhibit much less fragmentation at the same collision energy. The main ions are the non-dissociated molecular ion (*m/z* 46) and $C_2H_5O^+$ (*m/z* 45); a small amount of CH_2OH^+ (*m/z* 31) is also formed, the other prominent ions are then *m/z* 29 and *m/z* 27. However, isotopic labeling showed that their composition was $C_2H_5^+$ and $C_2H_3^+$, respectively. These ions are products of chemical reactions of the projectile radical cation with surface hydrogen of the CH-SAM surface: first, the protonated molecular ion $C_2H_5OH_2^+$ is formed by H-atom transfer and fragment ions $C_2H_5^+$, $C_2H_3^+$, or H_3O^+ result from its decomposition. These products of chemical reactions are not formed in the unimolecular decomposition of the ethanol molecular ion (see Figure 3c later on) and can be easily subtracted from the direct dissociation products of the projectile ion. (In this sense, the ethanol molecular ion has a great advantage over, e.g., hydrocarbon projectiles like $C_2H_6^+$, $C_3H_8^+$, or $C_4H_{10}^+$, where the direct dissociation products and products of chemical reactions, namely products of protonated molecular ion dissociation, are mixed.)

Figure 2c shows translational energy distributions of the major product ions from the $C_2H_5OH^+$–CF-SAM surface collisions at the incident energy of 22.6 eV (132_N = 60°, measured in the product ion angular maximum, Θ'_N = 75°). Most product ions are formed in strongly inelastic collisions with the surface, e.g., the maximum for the undissociated projectile ion is at 10 eV, about 40 % of the incident energy. If product ion energy distributions are converted to velocity (Figure 2d), the distributions for all product ions are very similar. This indicates that the decomposition of the surface-excited projectile ion occurs unimolecularly *after* the interaction with the surface. Figure 2e summarizes the velocity distributions of the product ions from $C_2H_5OH^+$–CH-SAM collisions. The similarity of the distributions for the inelastically scattered undissociated molecular ion

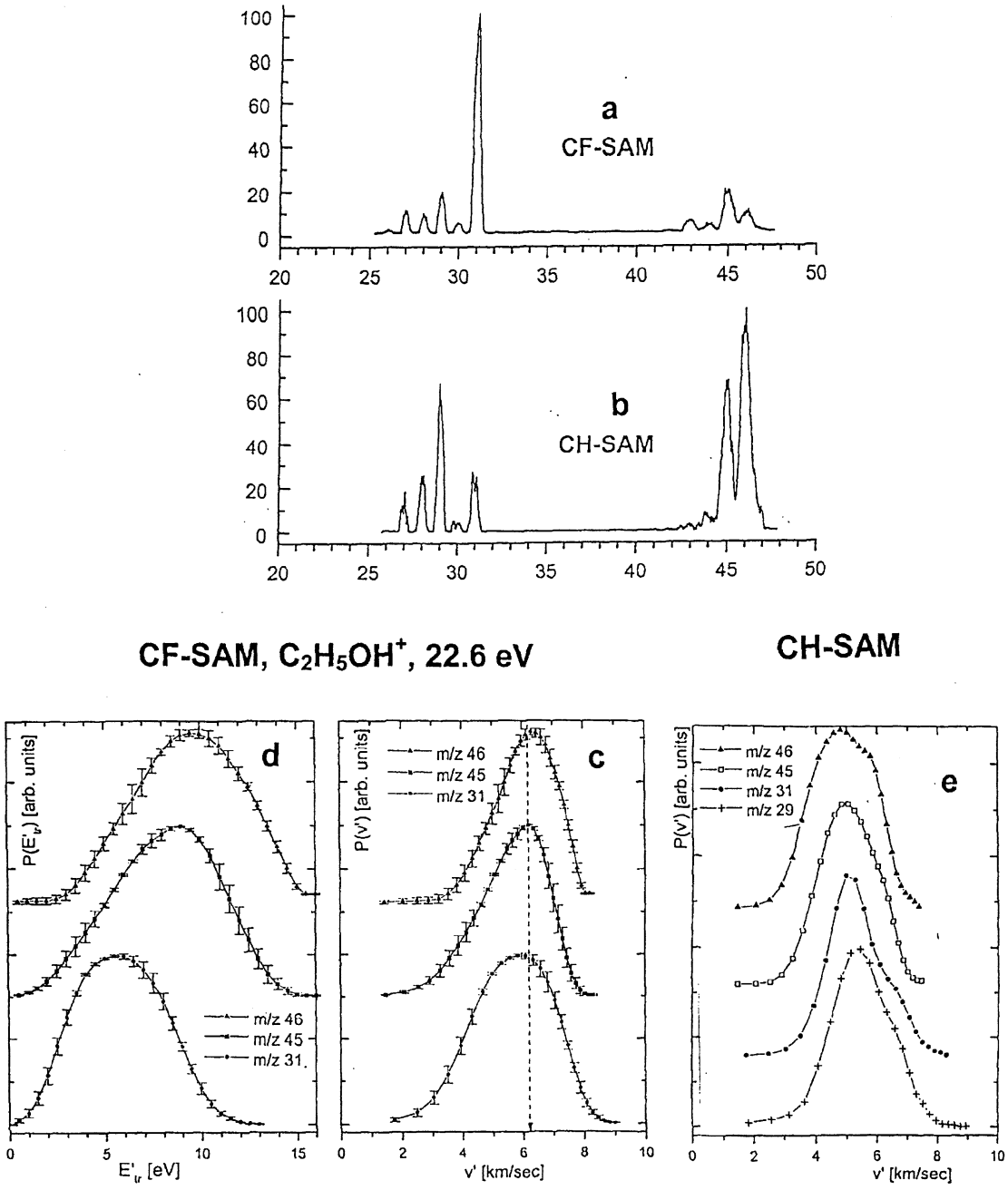

Figure 2. Examples of scattering data ($C_2H_5OH^+$, on a CF-SAM and CH-SAM surface, E_{tr} = 22.6 eV, Φ_N = 60°). (**a**) mass spectrum of ion products on CF-SAM; (**b**) mass spectrum of ion products on CH-SAM; (**c**) product ion (*m/z* 46, 45, 31) energy distributions in the angular maximum; (**d**) velocity distributions of product ions from (**c**); (**e**) velocity distributions of product ions (*m/z* 46, 45, 31, 29) on CH-SAM.

with those of the fragment ions leads to the same conclusion, namely, unimolecular decomposition of the excited molecular ion follows the interaction with the surface.

The fragmentation data were used to estimate the distribution of energy transformed into internal energy of the projectile ion in the surface collision, $P(E'_{int})$. The break-down pattern of the ethanol molecular ion is relatively well-known from both experimental and theoretical studies [15–17] and was used to deduce $P(E'_{int})$ by fitting the break-down graph to the relative intensities of the ion species in the mass spectra using trial functions for $P(E'_{int})$. An example of such a $P(E'_{int})$ estimation is given in Figure 3 for the collisions with the CF-SAM surface at two collision energies of 11.1 eV and 32.0 eV [13]. The lower part of the figure shows the

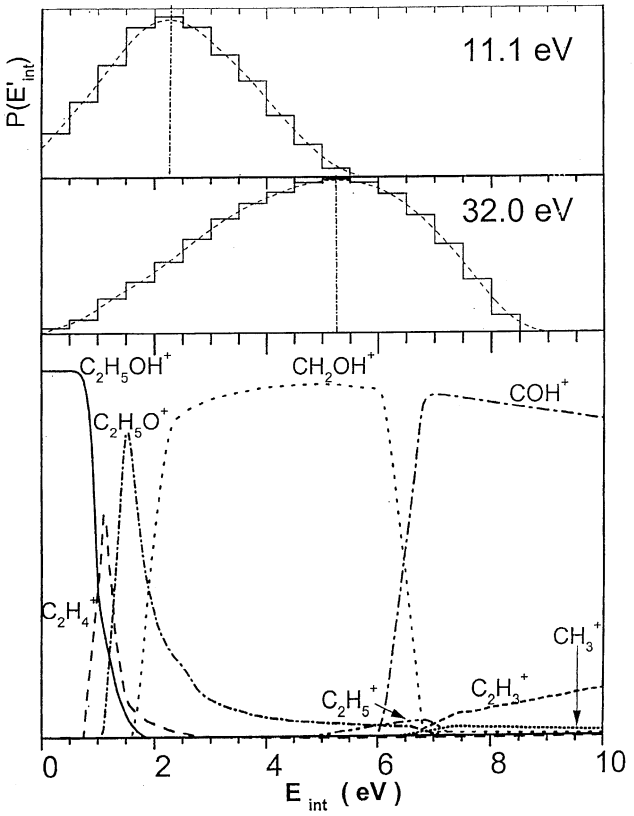

Figure 3. Distribution of energy transformed in the surface collision into the internal excitation of the projectile ion, $P(E'_{int})$, as obtained from the extent of the projectile ion fragmentation for incident energies of 11.1 eV and 32.0 eV. Data for $C_2H_5OH^+$ on a CF-SAM surface, $\Phi_N = 60°$, $\Theta'_N = 75°$ (angular maximum). Lower part shows the break-down pattern of the ethanol molecular ion used in the evaluation.

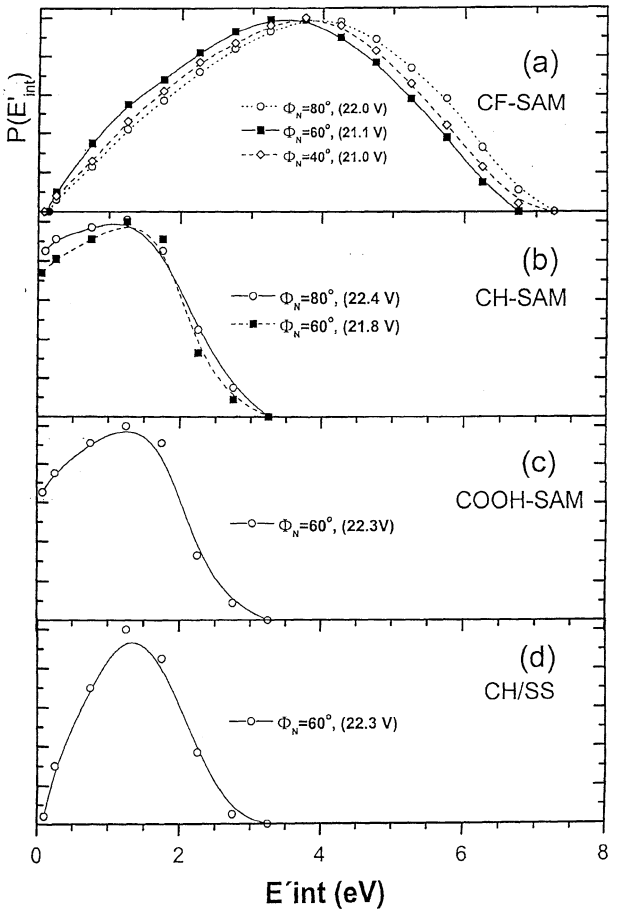

Figure 4. Distribution of energy transformed in the surface collision into the internal excitation of the projectile ion, $P(E'_{int})$, for various incident angles Φ_N on surfaces covered by (**a**) CF-SAM, (**b**) CH-SAM, (**c**) COOH-SAM, and (**d**) for hydrocarbon-covered stainless steel (CH/SS). Incident angle Φ_N and incident energies (in parentheses) are given in the figures. Mass spectra measured at the product ion angular maximum.

break-down pattern of the ethanol molecular ion. A comparison of $P(E'_{int})$ estimation for various SAM-surfaces (CF-SAM, CH-SAM, and COOH-SAM) and different incident angles Φ_N between 80° (i.e., close to the surface) and 40° of the projectile ions is given in Figure 4. In addition, the curve marked CH/SS indicates an earlier result [10] for hydrocarbon-covered metal target (stainless steel). It can be seen that at the same collision energy, $P(E'_{int})$ is similar for different incident angles between 40° and 80° for three surfaces (CH-SAM, COOH-SAM, and the CH/SS surface).

The only surface that showed a high translational-to-internal energy transfer was the CF-SAM surface (peak at 17% of the incident energy, in agreement with a value reported earlier [7]). The other surfaces showed a peak value at about 6% of the incident energy. This is smaller than obtained in other studies using thermometer molecules [18], but in fair agreement with recent data on fullerene ion–hydrocarbon-covered stainless steel collisions (6.8%) [19] and consistent with classical trajectory calculations for collisions of large polyatomic ions with CH-SAM surfaces [20]. The chemically modified CH-SAM behaved very similarly to surfaces covered by a layer of background hydrocarbons (stainless steel [13] or carbon [12]).

Figure 5 summarizes results on the translational-to-internal energy transfer for collisions of CD_4^+ radical cation with a carbon surface (HOPG) at room and at an elevated temperature [14]. At room temperature the surface was covered by a layer of background hydrocarbons, while at 1000 K the hydrocarbon layer was practically removed. Mass spectra for the unimolecular dissociation of the CD_4^+ projectile ions ($\Phi_N = 60°$, $\Theta'_N = 72°$) at three collision energies, 16.6, 31.6, and 51.6 eV were used, in combination with the break-down pattern of the methane molecular ion, to estimate the $P(E'_{int})$ for this system. This is not a very sensitive method for methane molecular ion, because the critical energies in the break-down pattern are widely separated and the relative concentrations of ions do not change much at excitation energies above 3 eV (Figure 5d). Consequently, the distribution functions $P(E'_{int})$ deduced using this fitting procedure should be regarded as

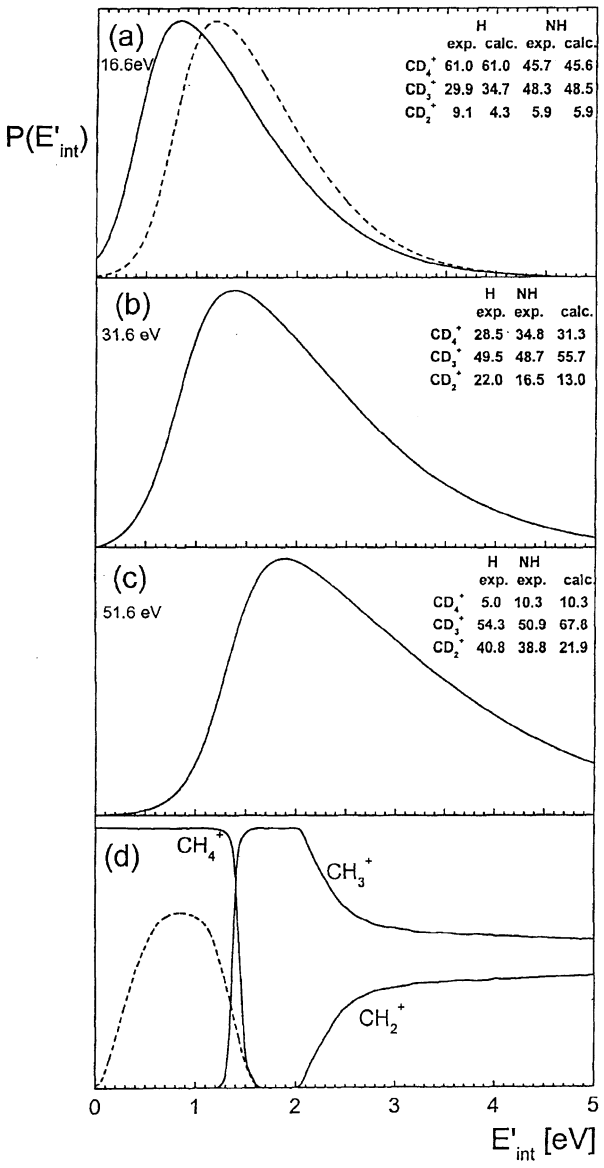

Figure 5. Distribution of energy transformed into the internal excitation of the projectile ion, $P(E'_{int})$, in surface collisions of CD_4^+ with heated (H) and room-temperature (NH, dashed) HOPG surfaces. Incident energy (**a**) 16.6 eV, (**b**) 31.6 eV, and (**c**) 51.6 eV, incident angle $\Phi_N = 60°$, measured in the angular maximum $\Theta'_N = 72°$; (**d**) break-down pattern of the molecular ion CD_4^+ used in the evaluation (dashed line: estimated distribution of initial internal excitation of CD_4^+). Numbers show comparisons of measured ion abundance with calculated abundance resulting from the fits.

approximate. An additional complication is that the projectile ion, when formed by electron impact, possesses a considerable amount of internal energy (estimated by the dashed curve in Figure 5d). The derived $P(E'_{int})$ curves exhibit tailing towards higher energies, but the mean energy transferred is again close to 5–6% of the incident energy and increases approximately linearly with increasing incident energy. The energy transfer was found to be practically the same for the surface at room temperature (collisions with the adsorbed hydrocarbon layer) and at the high temperature (collisions with C-atoms of the graphite surface). Only at the lowest collision energy (Figure 5a) there was a smal difference in the $P(E'_{int})$ curves; the mean value for the energy transfer on the heated surface seems to be by about 0.2 eV lower than on the room-temperature surface.

Incident Energy Partitioning

Data on incident energy partitioning in the surface collisions and dependence on the incident angle and incident ion energy were derived for different surfaces from the experimental data on fragmentation of the projectile ethanol molecular ion in surface collisions and on translational energy distributions of the product ions. The projectile ethanol molecular ion energy distribution was used as measured for the incident ion translational energy distribution, $P(E_{tr})$. The internal energy distribution of the projectile ion, $P(E_{int})$, was estimated as a product of the range of stability of the undissociated molecular ion, derived from its break-down pattern (see Figure 3), and the probability of populating internal energy states of the molecular ion in this range, obtained from tabulated ethanol photoelectron spectra. The term $P(E'_{tr})$ was taken as the measured translational energy distributions of the inelastically scattered undissociated molecular product ion. The distribution of energy transformed into the internal energy of the projectile ion, $P(E'_{int})$, was obtained from the extent of the surface-excited projectile ion fragmentation (see the preceding section). The distribution $P(E'_{surf})$ was taken as a difference of all these terms.

Figure 6 shows the data for energy partitioning in collisions of the ethanol molecular ion projectile (incident energy 21–22 eV) with the CF-SAM surfaces for three different projectile ions incident angles Φ_N. The results show that the fraction of energy, transformed into the internal energy of the surface-excited projectile ion, $P(E'_{int})$, was practically independent of the incident angle over the incident angle range of 10 to 50°, with a peak value of 17–18% of the incident energy and FWHM of about 4.1 eV (19% of the incident energy). The fraction of energy in product ion translation increased with the incident angle from the peak value of 16% at $\Phi_N = 40°$ to 52% of the incident energy at $\Phi_N = 80°$, with FWHM of 5–8 eV (22–36% of the incident energy). The distribution of the fraction of energy absorbed by the surface, $P(E'_{surf})$, correspondingly decreased from 66 to 30% of its peak value. Analogous dependence on the incident angle was observed for hydrocarbon-covered metal surfaces [10], though the distributions and peak values of the energy fractions were different (see also Figure 7 and Figure 8).

Figure 7 summarizes data on the dependence of the energy partitioning on the incident ion energy. The data shown refer to collision of the ethanol molecular ion with a hydrocarbon-covered stainless steel surface [10].

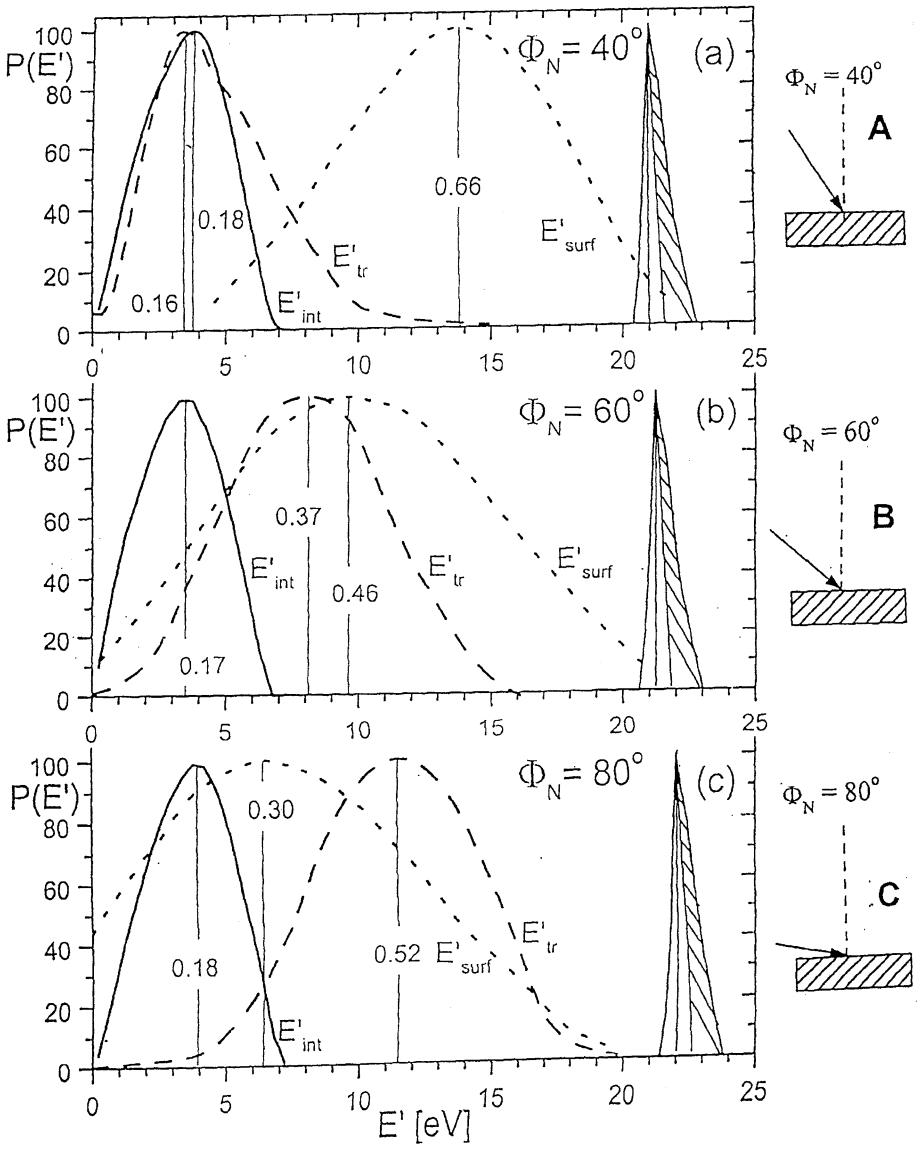

Figure 6. Distribution functions for energy partitioning into E'_{int}, E'_{tr}, and E'_{surf} from collisions of the ethanol molecular ion with the CF-SAM surface for incident projectile ion angle Φ_N (**a**) 40°, (**b**) 60°, and (**c**) 80°. Projectile incident energy 21–22 eV; measured at the angular maximum. Hatched area represents the estimated internal energy distribution of the projectile ion.

Over the incident energy range 13–33 eV (Φ_N = 60°) the energy partitioning practically did not change. The peak values of the fractions were the same within the experimental error and the particular distributions had a very similar shape. This indicates that the values of mean energy channeled into internal excitation, translational energy and the surface increased proportionally with increasing incident energy in the measured collision energy range. These conclusions are consistent with the results of classical trajectory simulations of collisions of $Cr(CO)_6^+$ with hydrocarbon SAM surfaces [21]. In the theoretical study the average value of E'_{int} was found to be about 8–10% and independent of the incident projectile energy. Also, the mean value of E'_{tr} and the width of its distribution at the incident energy of about 22 eV was in reasonable agreement with the experimental results reported here. However, in the theoretical study the average value of E'_{tr} was found to increase with the collision energy over 5–110 eV. The experiments did not show this decrease, however, in a much narrower collision energy window and on a slightly different hydrocarbon surface (Figure 7).

Finally, Figure 8 brings a comparison of energy partitioning in collisions of the ethanol molecular ion of the same incident energy (21–22 eV) and the same incident angle (Φ_N = 60°) with surfaces covered by different self-assembled-monolayers (CF-SAM, CH-SAM, and COOH-SAM) and, for comparison, with

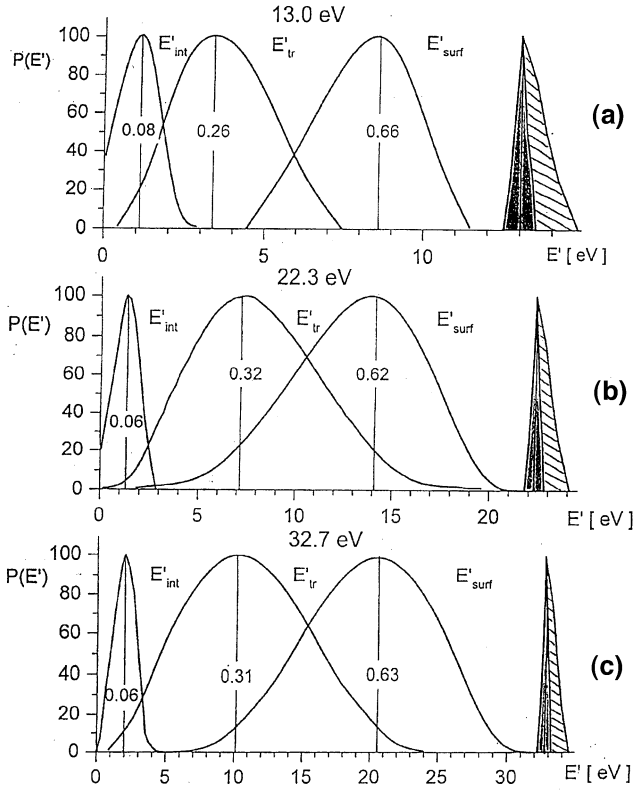

Figure 7. Distribution functions for energy partitioning into E'_{int}, E'_{tr}, and E'_{surf} from collisions of the ethanol molecular ion with the hydrocarbon-covered stainless steel surface for projectile ion incident energies (**a**) 13.0 eV; (**b**) 22.3 eV; (**c**) 32.7 eV. $\Phi_N = 60°$, measured in product ion angular maximum.

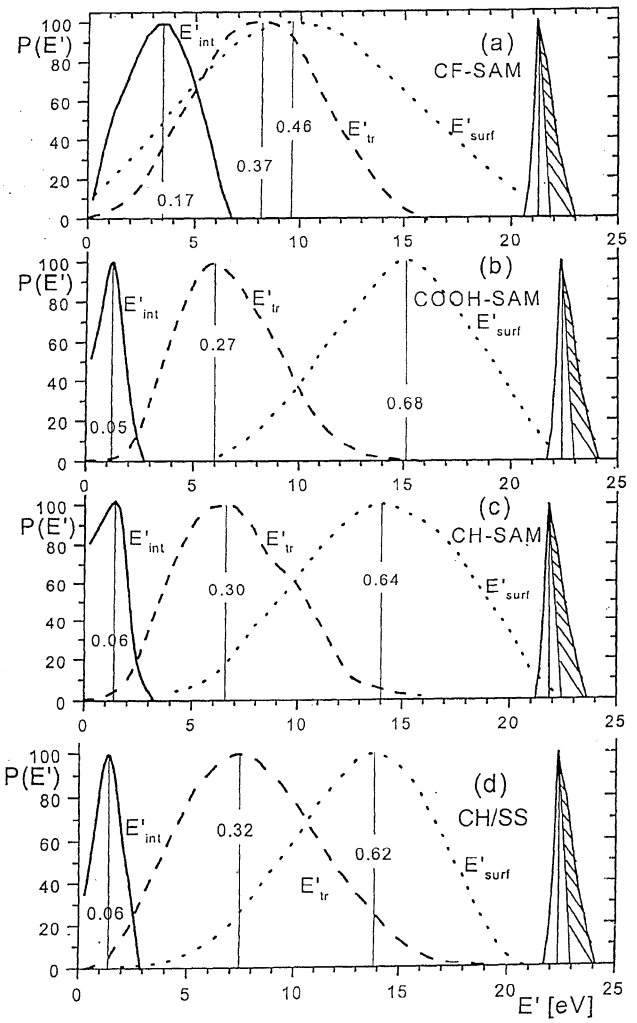

Figure 8. Comparison of distribution functions for energy partitioning into E'_{int}, E'_{tr}, and E'_{surf} from collisions of the ethanol molecular ion with (**a**) CF-SAM, (**b**) CH-SAM, (**c**) COOH-SAM, and (**d**) hydrocarbon-covered stainless steel surface (CH/SS). Incident energy 21.2–22.4 eV, incident angle $\Phi_N = 60°$, measured in the angular maxima ($\Theta'_N = 75°–70°$).

hydrocarbon-covered stainless steel surface [10]. It can be seen that the CH-SAM and the COOH-SAM surfaces give very similar results for energy partitioning to the hydrocarbon-covered stainless steel. The comparison between the CH-SAM and the hydrocarbon-covered stainless steel indicates that the self-assembled C_{12} hydrocarbon chain monolayer (CH-SAM) has very similar properties (as far as energy partitioning is concerned) to the random adsorbed layer of hydrocarbons on a stainless steel surface. The CF-SAM system is different in that the fraction of energy transformed into the surface-excited projectile internal energy is about 3-times higher than on the other surfaces in Figure 8 (peak value of 17% versus 5–6% of the incident energy, respectively). Also, the fraction of energy going into product ion translation appears to be larger for the CF-SAM surface and the fraction of energy absorbed by the surface correspondingly smaller (peak value of 40% for CF-SAM and 27–32% for CH-SAM and COOH-SAM of the incident energy).

Angular Distribution of Product Ions

Examples of polar plots of angular distributions of product ions from interaction of the ethanol molecular ions with the CF-SAM surface at the incident projectile ion energy of about 21 eV are given in Figure 9 [13]. The plots show the dependence on the incident angle. The figure also shows the dependence of the angular distribution of scattered CD_5^+ on hydrocarbon-covered HOPG on the collision energy. The angular distributions for all product ions tend to peak close to the same scattering angle and do not show any obvious correlation with the incident angle. For large incident angles (close to the surface) it is smaller than the specular angle, for smaller incident angles it tends to be larger than the specular angle. From a comparison of results on different surfaces [10, 12, 13] it appears that there is a correlation between the components of the velocities (maximum velocity of a distribution) of the incident and scattered ion in the angular maximum. The ratio of

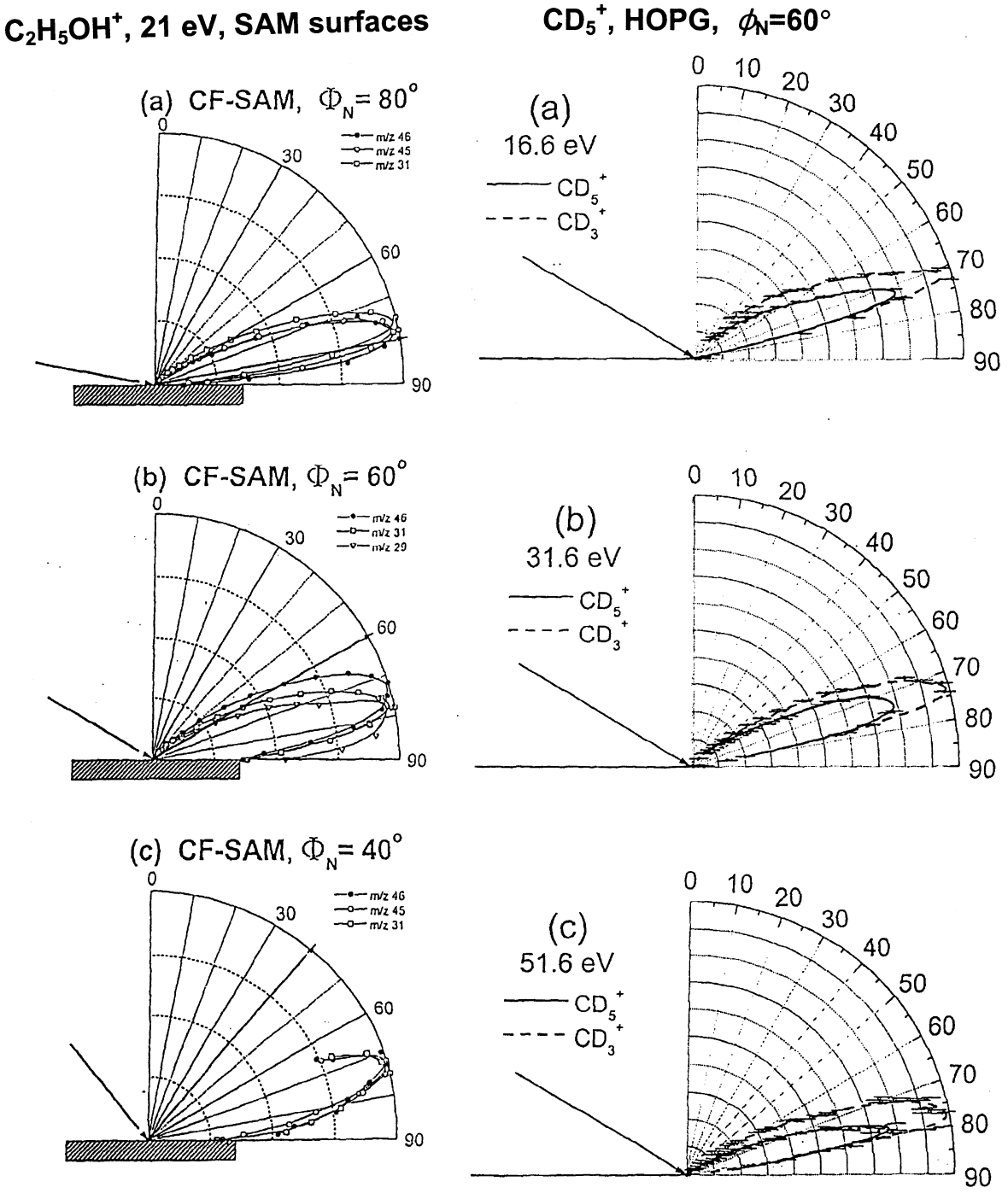

Figure 9. Angular distributions of product ions from ion-surface collisions. Left: Dependence on the incident angle for ethanol molecular ions on a CF-SAM surface, incident energy 21 eV, *m/z* of the product ions in insets (**a**) $\Phi_N = 80°$; (**b**) $\Phi_N = 60°$; (**c**) $\Phi_N = 40°$. Right: Dependence on the incident energy for CD_5^+ ions on hydrocarbon-covered HPPG, incident angle $132_N = 60°$, CD_5^+ solid line, CD_3^+ dashed (**a**) $E_{tr} = 16.6$ eV; (**b**) $E_{tr} = 31.6$ eV; (**c**)$E_{tr} = 51.6$ eV.

the most probable velocity components parallel to the surface of the scattered and incident ion appears to be independent of the incident angle and equal to 0.7. The value of the product ion velocity component perpendicular to the surface was almost constant and not dependent on the incident angle. However, it depended on the collision energy and also on the type of the surface studied [10, 13].

Measurements of both angular distributions and translational energy distributions of the product ions

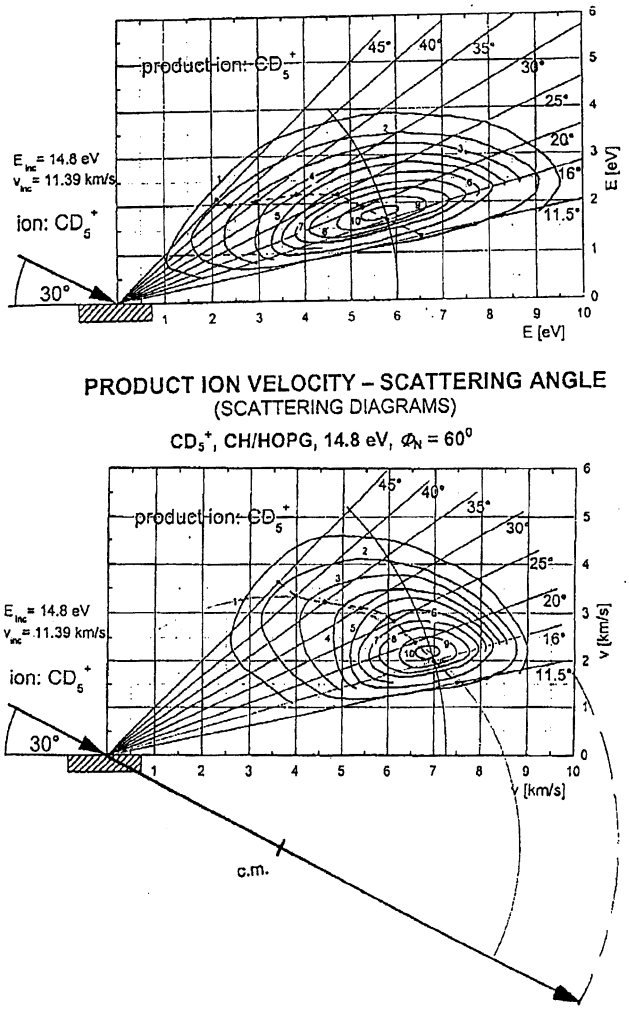

Figure 10. Contour scattering diagrams for CD_5^+ on hydrocarbon-covered HOPG surface, incident energy 14.8 eV, $\Phi_N = 60°$. Upper part: Dependence on scattered ion intensity on ion translational energy and scattering angle. Lower part: Dependence of scattered ion Cartesian probability (intensity divided by velocity) on ion velocity and scattering angle. Analysis: Incident laboratory velocity vector shifted to the scattering center; dashed circle: Loci of elastically scattered product ions; solid circle: Loci of inelastically scattered ions with c.m. located so that the circle would fit the maxima of distributions at the particular angles (solid points).

scattered after the interaction with the surface makes it possible to obtain scattering diagrams of the product ions, i.e., to construct contour diagrams of the dependence of the product ion flux on both the scattering angle and the product translational energy. Figure 10 shows such a dependence for the projectile ion CD_5^+ scattered on the carbon surface at room temperature (HOPG covered by a layer of hydrocarbons).

In analogy with gas-phase scattering, this diagram can be plotted also as a contour plot of the Cartesian probability of the product ion having a particular velocity at a scattering angle as a function of the ion velocity and scattering angle (see for example, [22, 23]). The Cartesian probability (here, ion intensity divided by ion laboratory velocity) shows the ion flux through a velocity space element $dv_x dv_y dv_z$ of the same size over the entire velocity space [22, 23]. The data from Figure 10a are plotted in this way in Figure 10b.

From the contour scattering diagram one can try to estimate the effective mass of the surface. Such an analysis is shown in Figure 10b. The incident ion laboratory velocity vector can be shifted to have its origin in the scattering center. This velocity vector represents here the relative velocity of the system incident ion (mass m_i – (stationary) effective surface area (unknown mass m_{eff}). The relative velocity vector is bisected by the effective center-of-mass (c.m.) proportionally to these masses of the colliding system. In case of *elastic* scattering of the incident ion, the scattered ion velocity should be located on a circle centered in the c.m. and going through the tip of the velocity vector (dashed circle in Figure 10b).

However, the scattering of CD_5^+ on the carbon surface is an *inelastic* event. For this case the recoil velocity of inelastically scattered CD_5^+ should be located on a circle of a smaller radius, but concentric with the elastic circle, if the inelastic energy loss does not depend on the scattering angle. Indeed, the peak values of the scattered ion laboratory velocity distributions for a series of scattering angles (solid points in the contour diagram) seem to form a ridge which is a part of a circle with a center on the velocity vector (marked c.m. in Figure 10b). The analysis [24], shown graphically in Figure 10b, leads to determining the position of the c.m. and from it to an effective mass of the surface $m_{eff} = 35 \pm 4$ m.u. A similar analysis of scattering of CD_5^+ on a HOPG surface, heated to 1000 K, leads to $m_{eff} = 55 \pm 5$ m.u. This is comparable to the mass of the terminal CH_3CH_2-group or two CH_3-groups on the hydrocarbon-covered carbon surface, and to about 4–5 carbon atoms of the hexagonal graphite face on the "naked" carbon surface. An analogous analysis of the scattering data has been carried out recently for dissociative collisions of ethanol molecular ions on a fluorinated alkylthiol surface (estimated m_{eff} about 100 m.u.) [25].

Ion Survival Probability

The fraction of ions surviving the surface collision was determined from the intensity of the projectile ion striking the surface and from the sum of intensities of the product ions and their angular distributions. The absolute values of ion survival probability, estimated in this way, showed a large difference in the survival of radical cations and closed-shell ions of low recombination energy. For instance, the survival probability of CD_5^+ (energy range 15–50 eV, incident angle $\Phi_N = 60°$) on a hydrogen-covered carbon (HOPG) surface was found to be about 12% [13], while that one of the radical cation CD_4^+ was only about 0.3 % [13]. Similarly, the

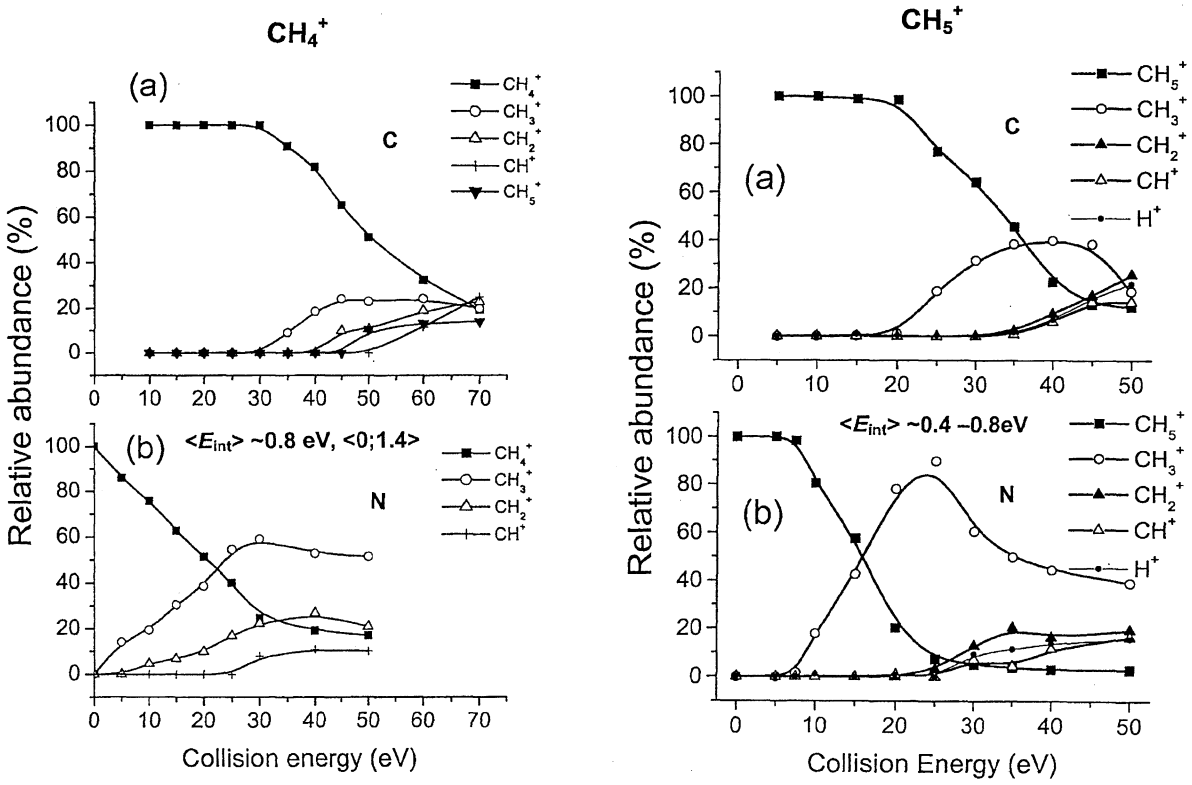

Figure 11. Effect of internal energy of projectile ions: Dependence of product ion intensities on projectile ion incident energy (CERMS curves) for projectile ions formed (**a**) in the Colutron source (C) and (**b**) in the Nier-type source (N). Incident angle 45°, scattering angle 45°. Left: Incident ion CH_4^+, right: Incident ion CH_5^+. Product ion designation in insets, $<E_{int}>$ in (**b**): Estimated internal energy content.

survival probability of the radical cation $C_2H_5OH^+$ on a hydrocarbon-covered stainless-steel surface was found more than 10-times lower than that of closed shell ions $C_2H_5OH_2^+$ or $C_2H_5O^+$ [10]. The survival probability depended strongly on the incident angle: For the above mentioned ions $C_2H_5OH^+$, $C_2H_5OH_2^+$, and $C_2H_5O^+$ it was found to increase about 100× when going from a steep impact angle ($\Phi_N = 40°$) to collisions close to the surface parallel ($\Phi_N = 80°$) [10].

Internal Energy of Projectile Ions

Most of the terms of eq 1 which determine energy partitioning in a polyatomic molecular ion colliding at low collision energy with a surface were discussed in the previous sections. The only remaining energy term is the initial internal energy of the projectile ion, E_{int}. The two limits are that the initial internal energy of the projectile may be preserved during the surface collision to drive further dissociation of the surface excited projectile, or that E_{int} may be fully equilibrated with surface modes during the collision. Everything between these limits is possible, in principle. For most of the previous studies described here, E_{int} was low (ethanol molecular ion) and thus its specific effect is expected to be rather small.

In our recent experiments [26], the effect of the initial internal energy of projectile ions on the extent of fragmentation was investigated. The experiments were carried out on a special ion-surface collision apparatus BESTOF in Innsbruck [27] and consisted in measuring mass spectra of ion products resulting from surface-induced dissociation of simple polyatomic projectiles as a function of collision energy (collision-energy-resolved mass-spectra, or CERMS curves). The projectile ions were simple hydrocarbon ions prepared in two different sources, either by electron impact under quasi-single collision conditions (Nier-type source) or in a multi-collisional Colutron source. In the former case, initial internal energy of the ion from the ionization process should be preserved, in the latter case, substantial collisional relaxation of the ion could take place.

Figure 11 shows as an example the CERMS curves of product ions from collisions of the CH_4^+ radical cation and the CH_5^+ closed-shell ion with a hydrocarbon-covered stainless steel surface. The ion intensities are normalized to the sum of all product ion intensity. Clearly the extent of fragmentation of the projectile ions formed in two different ways is quite dissimilar. For the projectile ions formed in the Nier-type source (N), with

initial internal energy preserved, characteristic features in the CERMS curves (thresholds of fragment ion formation, characteristic crossings between intensities of different ion species) occur at much lower collision energies than for the projectile ion from the Colutron source (C). The shifts for CH_4^+ are about 30–40 eV. If one takes for the efficiency of the translational-to-internal energy transfer on this surface the well-established value of 6% this energy difference would be comparable to additional internal energy of approximately 1.5 eV. This is about the upper value of internal energy expected in undissociated ion CH_4^+ formed by electron impact (estimated in Figure 5). Similarly, the shift of thresholds and crossings in the CERMS curves for CH_5^+(N) and CH_5^+(C) projectile ions is about 15–20 eV and this would correspond to the effect of internal energy difference of about 1 eV. It appears, thus, that the projectile ions CH_5^+ from the Colutron source were practically relaxed. These data are consistent with the hypothesis that the internal energy of the projectile ions is preserved during the ion-surface collision and available for further dissociation of the surface-excited projectile.

Acknowledgments

The studies described in this paper were carried out by the author in collaboration with his former graduate students and Prague colleagues J. Žabka, J. Roithová, J. Kubišta, Z. Dolejšek, J. Jašík, and I. Ipolyi, all cited as co-authors of the papers in references. Part of the research resulted from collaboration with the group of T.D. Märk, Institute for Ion Physics, Leopold-Franzens University, Innsbruck. The section on the effect of projectile internal energy is based on results obtained in Innsbruck by the authors of reference [26, 27]. The author expresses his thanks and appreciation to all the collaborators. The author also gratefully acknowledges partial support of this research by grants of the Grant Agency of the Czech Republic 203/97/0351 and 203/00/0632, by the Association EURATOM-IPP.CR in collaboration with Association EURATOM-ÖAW, and by the grants Kontakt 2000-06, ME188 and ME 561 of the Ministry of Education, Youth, and Sports of the Czech Republic.

References

1. Rabalais, J. W. Low Energy Ion-Surface Interactions; J. Wiley: New York, 1994, p 313.
2. Cooks, R. G.; Ast, T.; Mabud, M. D. Collisions of polyatomic ions with surfaces. *Int. J. Mass Spectrom.* **1990,** *100,* 209.
3. Hanley L. Polyatomic Ion-Surface Interactions. Int. J. Mass Spectrom. **1998,** *174,* 1.
4. Grill, V.; Shen, J.; Evans, C.; Cooks, R. G. Collisions of Ions with Surfaces at Chemically Relevant Energies: Instrumentation and Phenomena. *Rev. Sci. Instrum.* **2001,** *72,* 3149.
5. Kenttämaa, H. I.; Cooks, R. G. Internal Energy Distributions Acquired Through Collisional Activation at Low and High Energies. *Int. J. Mass Spectrom. Ion Processes* **1985,** *64,* 79.
6. Vékey, K.; Somogyi, A.; Wysocki, V. *J. Mass Spectrom.* **1995,** *95,* 212.
7. Wysocki, V. H.; Kenttämaa, H. I.; Cooks, R.G. Internal Energy Distributions of Isolated Ions After Activation by Various Methods. *Int. J. Mass Spectrom. Ion Processes* **1987,** *75,* 181.
8. Wainhaus, S. B.; Gislason, E. A.; Hanley, L. Determination of Activation Energies for Ion Fragmentation by Surface-Induced Dissociation. *J. Am. Chem. Soc.* **1997,** *119,* 4001.
9. Meroueh, O.; Wang, Y.; Hase, W. L. Direct Dynamics Simulation of Collision- and Surface-Induced Dissociation of N-Protonated Glycine. Shattering Fragmentation. *J. Phys. Chem. A* **2002,** *106,* 9983 and references cited therein.
10. Kubišta, J.; Dolejšek, Z.; Herman, Z. Energy Partitioning in Collisions of Slow Polyatomic Ions with Surfaces: Ethanol Molecular Ions on Stainless Steel Surfaces. *Eur. Mass Spectrom.* **1998,** *4,* 311.
11. Wörgötter, R.; Kubišta, J.; éabka, J.; Märk, T. D.; Herman, Z. Surface Induced Reactions and Decompositions of the Benzene Molecular Ion $C_6H_6^+$: Product Intensities, Angular and Translational Energy Distributions. *Int. J. Mass Spectrom. Ion Processes* **1998,** *174,* 53.
12. Žabka, J.; Dolejšek, Z.; Roithová, J.; Grill, V.; Märk, T. D.; Herman, Z. Energy Partitioning in Collisions of Slow Polyatomic Ions with Carbon Surfaces. *Int. J. Mass Spectrom.* **2002,** *213,* 145.
13. Žabka, J.; Dolejšek, Z.; Herman, Z. Energy Partitioning in Collisions of Slow Polyatomic Ions with Surfaces: Ethanol Molecular Ions on Surfaces Covered by Self-Assembled Monolayers (CF-SAM, CH-SAM, COOH-SAM). *J. Phys. Chem. A* **2002,** *106,* 10861.
14. Roithová, J.; Žabka, J.; Dolejšek, Z.; Herman, Z. Collisions of Slow Polyatomic Ions with Surfaces: Dissociation and Chemical Reactions of CD_5^+, CD_4^+, and CD_3^+ and Their Isotopic Variants on Room-Temperature and Heated Carbon Surfaces. *J. Phys. Chem. B* **2002,** *120,* 8293.
15. von Koch, H.; Lindholm, E. Dissociation of Ethanol Molecule Ions Formed in Charge Exchange Collisions with Positive Ions. *Ark. Fyz.* **1961,** *19,* 123.
16. Niwa, Y.; Nishimura, T.; Tsuchia, T. Ionic Dissociation of Ethanol Studied by Photoelectron-Photoion Coincidence Spectroscopy. *Int. J. Mass Spectrom. Ion Phys.* **1982,** *42,* 91.
17. Friedman, l.; Long, F. A.; Wolfsberg, M. Study of Mass Spectra of Lower Aliphatic Alcohols. *J. Chem. Phys.* **1957,** *27,* 613.
18. Miller, S. A.; Riederer, D. R.; Cooks, R. G.; Cho, W. R.; Lee, H. W.; Kang, H. Energy Disposal and Target Effects in Hyperthermal Collisions of Ferrocene Molecular Ions at Surfaces. *J. Phys. Chem.* **1994,** *98,* 245.
19. Biasioli, F.; Fiegele, T.; Mair, C.; Herman, Z.; Echt, O.; Aumayr, F.; Winter, HP.; Märk, T. D. Surface-Induced Dissociation of Singly- and Multiply-Charged Fullerene Ions. *J. Chem. Phys.* **2000,** *113,* 5053.
20. Merouh, O.; Hase, W. L. Effects of Surface Stiffness on the Efficiency of Surface-Induced Dissociation. *Phys. Chem., Chem. Phys.* **2001,** *2,* 2306.
21. Song, K.; Meroueh, O.; Hase, W. L. Dynamics of $Cr(CO)_6^+$ Collisions with Hydrogenated Surfaces. *J. Chem. Phys.* **2003,** *118,* 2893.
22. Friedrich, B.; Herman, Z. Processing of Ion-Molecule Beam Scattering Data: Framework of Scattering Diagrams and Derived Quantities. *Collection Czech. Chem. Commun.* **1984,** *49,* 570.
23. Herman, Z. The Crossed-Beam Scattering Method in Studies of Ion-Molecule Reaction Dynamics. *Int. J. Mass Spectrom.* **2001,** *212,* 413.
24. Ipolyi, I.; Jašík, J.; Žabka, J.; Roithová, J.; Herman, Z., unpublished.

25. Shukla, A.; Futrell, H. H. Dynamics of Hyperthermal Energy Ion-Surface Collisions: Dissociation and Non-Dissociative Scattering of Ethanol Cations from SAM Surface of Fluorinated Alkylthiol on Au(111). *Int. J. Mass Spectrom.* **2003,** *223/224,* 783.
26. Qayyum, A.; Tepnual, T.; Mair, C.; Matt-Leubner, S.; Scheier, P.; Herman, Z.; Märk, T. D. The Role of Internal Energy of Polyatomic Projectile Ions in Surface Induced Dissociation. *Chem. Phys. Lett.* **2003,** *376,* 539.
27. Qayyum, A., Herman, Z., Tepnual, T., Mair, C., Matt-Leubner, S., Scheier, P., Märk, T. D. Surface Induced Dissociation of Polyatomic Hydrocarbon Projectile Ions with Different Initial Internal Energy Content, unpublished.